Published in final edited form as:
Biol Bull. 2011 April ; 220(2): 89–96.

Isolation and Ultrastructural Characterization of Squid Synaptic Vesicles

Gulcin Pekkurnaz[1,4,1], **Andrea Fera**[2,4], **Jessica Zimmerberg-Helms**[1,4], **Joseph A. DeGiorgis**[2,3,4], **Ludmila Bezrukov**[1], **Paul S. Blank**[1], **Julia Mazar**[1,4], **Thomas S. Reese**[2,4], and **Joshua Zimmerberg**[1,4]

[1]National Institute of Child Health and Human Development, NIH, Bethesda, MD 20892

[2]National Institute of Neurological Disorders and Stroke, NIH, Bethesda, MD 20892

[3]Biology Department, Providence College, Providence, RI 02918

[4]Marine Biological Laboratory, Woods Hole, MA 02543

Abstract

Synaptic vesicles contain a variety of proteins and lipids that mediate fusion with the pre-synaptic membrane. Although the structures of many synaptic vesicle proteins are known, an overall picture of how they are organized at the vesicle surface is lacking. In this paper, we describe a better method for the isolation of squid synaptic vesicles, and characterize the results. For highly pure and intact synaptic vesicles from squid optic lobe, glycerol density gradient centrifugation was the key step. Different electron microscopic methods show that vesicle membrane surfaces are largely covered with structures corresponding to surface proteins. Each vesicle contains several stalked globular structures extending from the vesicle surface that are consistent with the V-ATPase. BLAST search of a squid EST library identifies 10 V-ATPase subunits, which are expressed in the squid stellate ganglia. Negative stain tomography demonstrates directly that vesicles flatten during the drying step of negative staining, and furthermore shows details of individual vesicles and other proteins at the vesicle surface.

Introduction

Neurotransmitter release by fusion of synaptic vesicles with the pre-synaptic plasma membrane upon transient increases in intracellular Ca^{2+} is essential for propagating action potentials between neurons. Synaptic vesicle (SV) fusion requires cooperative interactions between the lipids and proteins of both the pre-synaptic and SV membranes. Although the structure of many SV proteins have been solved and a prototypic structural model of an individual SV has been presented (Takamori et al., 2006), an overall picture of how proteins are organized at the vesicle surface is still lacking.

It is well established that the vertebrate and invertebrate nervous systems exhibit many similarities in terms of neuronal function. The squid nervous system in particular has been used to demonstrate the neuronal resting potential as well as to record electrical action potentials. The squid was also used to define the role of calcium in synaptic transmission. The squid optic lobe contains 50-80% of the neurons in the squid central nervous system and is therefore an excellent source of synaptic vesicles to study their biophysical and structural properties. Dowdall and Whittaker (1973) described the isolation of synaptic vesicle rich

Correspondence to J. Z.: joshz@mail.nih.gov.
[1]Present address: The F.M. Kirby Neurobiology Center, Children's Hospital, Boston, MA 02115, USA.

fractions from squid optic lobe by osmotic shock. However, the purity of their final fraction was never critically evaluated either by biochemical techniques or electron microscopy (Dowdall and Whittaker, 1973). Chin and Goldman used the same method to purify synaptic vesicles from frozen squid optic lobe and added controlled-pore glass chromatography as a final purification step. Based on their detailed biochemical analysis, the vesicle fraction was approximately 60% pure (Chin and Goldman, 1992).

Using advances in the purification of synaptic vesicles from rat brain (Huttner *et al.*, 1983), a SV isolation protocol for squid (*Logilo pealei*) optic lobe was optimized in this study to obtain a highly pure and intact SV population for biochemical and ultrastructural studies. The SV-enriched fractions were analyzed to evaluate their purity and size distribution by electron microscopy (EM), as well as the effects of different EM specimen preparation techniques on the average SV size. The distribution of SV size in SV-enriched fractions suggests that the SV we isolated are more than 95 percent pure. Finally, the purified vesicles were used to characterize the organization of the surface of individual SVs by tungstate-based negative stain EM tomography. Here we present a three-dimensional molecular rendering of the surface structure, presumably V-ATPase, reflecting an individual SV, rather than the average of many SV.

Materials and Methods

Preparation of synaptosomes

Live squid (*Loligo pealei*) obtained from the Marine Resources Center, Marine Biological Laboratory, Woods Hole, Massachusetts were maintained for 2 to 24 hr in tanks containing running seawater at 16-22°C. All further manipulations were in ice-cold buffers containing 0.01% 2,6-Di-*tert*-butyl-4-methylphenol (BHT) to prevent lipid oxidation. Squid optic lobes were dissected onto pre-chilled Petri dishes and weighed. Synaptosomal fractions were prepared as previously described (Dowdall and Whittaker, 1973, Pollard, 1975), with modification to produce an isotonic homogenization buffer [1M sucrose, 5mM HEPES, 10mM EDTA/EGTA pH 7.4 with protease inhibitor cocktail (Roche Applied Science, Indianapolis, IN)]. Squid optic lobes were homogenized as a 20% (w/v) solution in 1M sucrose buffer by 6-8 complete strokes of a glass-on-glass TenBroek homogenizer with pestle B. The homogenate (H) was centrifuged at 13,000g for 1 hr at 4°C in a JA-20 rotor. The latter step yielded a pellet (P1; mitochondrial fraction), a floating particulate layer (PL; synaptosomal fraction), and an opaque supernatant (S1; microsomal fraction, Fig 1A). The synaptosomal fraction was collected and stored on ice for further fractionation.

Purification of synaptic vesicles

The synaptosomal fraction was diluted in ice-cold distilled water supplemented with protease inhibitor cocktail (Roche Applied Science, Indianapolis, IN) (2ml/g of synaptosomal tissue), and then resuspended with a glass Pasteur pipette. The synaptosomal lysate (L) was adjusted with 10mM HEPES (pH 7.3) and 10mM EDTA and incubated for 20 min, followed by centrifugation at 21,000g for 20 min. The supernatant (LS1) was collected and centrifuged at 195,000g for 2h.

The pellet (LP2) containing the crude SV fraction was re-suspended in 0.4M sucrose and homogenized by passing through a 25 gauge needle (10 times). The re-suspended vesicles were layered on to a sucrose step gradient (0.4, 0.6, 0.8, 1 and 1.2M sucrose) and centrifuged for 2 hr at 54,000g using a Beckman SW41Ti swing-bucket rotor. Purified SVs concentrated in the 0.4M sucrose band (SG-V), was aspirated, diluted into squid 1/2X buffer (175mM aspartic acid, 65mM taurine, 85mM betaine, 25mM glycine, 10mM HEPES, 6.5mM Mg_2Cl, 5mM EGTA pH 7.2) and centrifuged at 198,000g for 1 hr to obtain vesicle

pellet. Synaptic vesicle pellet (SVP) resuspended with squid 1/2X buffer, was homogenized by passing through a 25 gauge needle and then loaded onto a continuous glycerol gradient (Clift-O'Grady et al., 1990).

Immunoblots

Bicinchoninic acid (BCA) assay kits (Thermo Scientific, Pierce Biotechnology, Rockford, lL) were used to measure total protein concentration in fractions, using bovine serum albumin (BSA) as a standard. Samples were boiled in gel loading buffer containing 5% 2-mercaptoethanol (Sigma Chemical Co., St. Louis, MO), and immediately transferred to ice. SDS-PAGE was carried out using 4-20% tris-glycine Gel (NOVEX, San Diego, CA), and 5 μg of total protein/sample. Proteins were transferred to PVDF membranes (0.2 μm pore size). Blots were blocked in phosphate-buffered saline (PBS), pH 7.2, containing 5% non-fat milk and 0.05% Tween-20 for 1 hr with gentle agitation. Anti-SNAP-25 (Alomone Labs Ltd., Jerusalem, Israel) and anti-VDAC (*N18*; Santa Cruz Biotechnology, Inc., Santa Cruz, CA) antibodies were diluted in block (1:1000), and blots were probed for 60 min. Blots were rinsed 4×15 min in PBS-0.05%Tween-20 (PBST) and then incubated in alkaline phosphatase-conjugated secondary antibodies diluted in block (1:8000) for 1 hr. Blots were rinsed in PBST for 4×15 min with agitation and developed with ECF substrate (GE Healthcare UK Limited, Little Chalfont Buckinghamshire, UK). Blots were visualized using a Fujifilm FLA-3000 scanner, and band intensities quantified using Image Gauge software, version 3.46, FUJI PHOTO Film Co. LTD.

Sample preparation for electron microscopy

Chemical fixation—Synaptosomal fractions were centrifuged at 10,000 × g for 5 min in 1% BSA to form a sticky pellet. Pellets were fixed in 3% glutaraldehyde, 0.5% acrolein (1:2; synaptosomal pellet/fixative) and post-fixed in 1% osmium in water. Fixed pellets were washed with 0.1M sodium acetate buffer (3x), and 1M sucrose (x1), dehydrated through a series of ethanol solutions, embedded in araldite, sectioned and stained conventionally.

Negative Stain—10μl drops of each SV fraction were placed on parafilm in a covered, humidified Petri dish. Freshly glow discharged, Formvar coated, 400 mesh, copper grids (SPI Supplies) were incubated for 10 min on the SV drops, washed 3 × 10 min in squid 1/2X buffer and stained with 1% uranyl acetate in water.

Cryofixation—The synaptosomal fraction and SV fractions respectively were centrifuged at 13000 × g for 5min and 198,000 × g for 1h in 1%BSA. Samples were rapid-frozen with a Life Cell CF-100 freeze-slam apparatus (Life Cell; The Woodlands, TX), freeze substituted (Petersen et al., 2003), embedded and thin sectioned. Sections were stained routinely with uranyl acetate and lead citrate.

Tomography

Freshly glow-discharged copper grids coated with Formvar and carbon were floated on drop of synaptic vesicle preparation. Fiduciary markers were then added by floating the grids for 10 min on a 10 μl drop of goat anti-rabbit antibody linked to 10 nm gold (Ted Pella Inc., Redding, CA). Finally, grids were negative stained by floating them for one minute on a 10 μl drop of 2.0% methylamine tungstate (NanoW; www.nanoprobes.com/Inf2018.html). Tomography series were collected at 300 KV in a Tecnai TF30 transmission electron microscope, equipped with a 2,048 X 2,048 pixels Ultrascan, charge-coupled device (CCD) camera from Gatan at a pixel size of 0.29 nm. Images were collected at each 2° of tilt ±60° in orthogonal X and Y axes. NanoW is unchanged by the radiation from this tomography protocol (Fera A., unpublished).

Images from each axis were aligned separately to sub-pixel accuracy using IMOD with the 10-nm gold particles serving as fiduciary markers (Kremer et al., 1996). The two tilt series were then combined into a tomogram at an accuracy of 0.3 pixels, the upper limit for the acceptable residual warping error in IMOD. Virtual sections, one voxel thick, were derived from the tomograms and then binned by two for further examination. ImageJ (http://rsb.info.nih.gov/nih-image/) was used to display virtual sections for evaluation and measurement. Data was spatially filtered and modified only for brightness and contrast.

Morphometric analysis of synaptic vesicles

Images were collected with a CCD digital camera system (XR-100 from AMT, Danvers, MA) at a microscope magnification of 40,000× and examined using the public domain NIH Image program; ImageJ (http://rsb.info.nih.gov/nih-image/).

Identification of V-ATPase transcripts in squid neuronal tissues

Previously, we have generated a squid EST database by single-pass sequencing 22,689 cDNA clones derived from mRNA of the squid stellate ganglia, *Loligo pealei* (DeGiorgis et al, submitted). These “expressed sequence tags” were assembled into contigs and singletons to yield 10,027 unique sequences and each sequence analyzed by BLASTX. Resulting analysis was scanned for subunit transcripts that are known to contribute to the functional V-ATPase. This data is represented in Table 2.

Results

Characterization of the synaptic vesicle enriched fraction

The purification procedure using homogenization of tissue, differential centrifugation, sucrose gradient flotation and chromatography on a controlled glass pore column provided a SV-enriched fraction of 60% purity (Chin and Goldman, 1992). In order to obtain intact vesicles with higher purity, freshly dissected optic lobe tissue was further fractionated by continuous glycerol density gradient centrifugation (Fig 1A). The density of closed vesicles on density gradients of membrane impermeable solutes, such as sucrose, differs from the density measured using the density gradient of membrane permeable substances such as glycerol (Carlson et al., 1978). A vesicle peak obtained after the glycerol gradient was enriched in a homogeneous population of intact vesicles (Fig 1B and C), within which membrane pieces and large microsomes were very rare.

A SNAP-25 antibody was used to probe Western blots of fractions obtained during the purification steps, revealing a single band of immunoreactivity at ~30kDa (Fig 1D). Comparison of subcellular fractions indicated that SNAP25 was enriched in the synaptosomal fraction (PL) compared to the initial homogenate (H). SNAP-25 was present in the synaptic vesicle fractions but not enriched relative to the other fractions, in conformity with observations on rat brain (Takamori et al., 2006). However, the vesicle peak obtained following the glycerol gradient showed SNAP-25 enrichment relative to the other fractions. SV rich fractions of rat brain contain the SV integral membrane proteins Synaptotagmin and SV2 as well as SNAP-25 (Kretzschmar et al., 1996). Other synaptic vesicle proteins could not be analyzed due to the lack of suitable antibodies. VDAC protein was used as a mitochondrial marker to demonstrate that there is no detectable mitochondria contamination even in the crude SV fraction (LP2) (Fig 1D). As expected, the recovery of SV enriched fraction is low (0.03 ± 0.01, n=4) due to the osmotic shock treatment and further fractionation with glycerol, a membrane permeable solute used to eliminate broken vesicles (Table 1). Yields were ~ 0.3 mg of SV from 11 g of optic lobe tissue, from 40-50 squid. We further evaluated the purity of this fraction based on SV diameter measurements.

The outer diameter has been traditionally used as a metric for SV size. Here, we measured the diameter of SV by outlining the outer SV membrane and then calculated the longest distance between any two points along the selection boundary (Feret's diameter). In addition, we determined circularity by using the built-in routines found in ImageJ software. Each vesicle counted had a clear membrane border and distinct negative staining. The calculated circularity value was >0.998 (n=5000), indicating that the SV were uniform in their horizontal and vertical dimensions. We further evaluated the probability distribution of measured diameters to assess the level of contamination. A single Gaussian fit of the frequency histogram was used to calculate mean SV diameter and standard deviation. Values larger than the mean plus four standard deviations (99.994% confidence interval) were taken as an indication of contamination of the SV fraction, and results show that the purity of the SV enriched fraction was 96 ± 2.6% (mean±SD, n=20 different isolations). The same analysis was performed for area and volume values. There was no significant difference between the three types of analysis; therefore we used the diameters as a measure for SV size.

Effect of specimen preparation method on synaptic vesicle diameter

Accurate assessment of SV size within pre-synaptic nerve terminals and in SV-enriched fractions requires sample preparation for electron microscopy and morphometric analysis. The size distribution of synaptic vesicles at intact nerve endings (synaptosomes) and within SV-enriched fractions was compared using different preparation techniques to determine precisely the mean diameter of SV (Fig 2). Our morphometric analysis results revealed that the vesicle size distribution was significantly different according to sample preparation technique (ANOVA, $p<0.001$, Fig 2). The outer diameter of SV in synaptosomes, excluding dense core vesicles, was compared. In fixed and rapid-frozen synaptosome samples, mean diameters were 47.8 ± 0.7 nm (mean ± SEM, n=142) and 52.1 ± 0.8 nm (mean ± SEM, n=125), respectively. Shrinkage during aldehyde fixation as well as rounding and swelling of vesicles due to subtle ice crystal formation during rapid freezing could explain a small difference in SV diameter differences (Student's t-test, $p<0.001$). A visible pellet of the SV-enriched fraction was used to prepare a rapid-frozen sample, which revealed a SV diameter of 50.1 ± 0.8 nm (mean ± SEM, n=125), very similar to the value obtained from SV in slam-frozen synaptosome samples.

For further evaluation, the size distributions of freshly isolated, negatively stained (with uranyl acetate) SVs were compared to other samples. Negative staining theoretically replaces water in the interstices of the object until all hydrated volumes are filled with stain, thus forming a uniformly thin, amorphous film in which the specimen is supported and preserved. Negative stained samples had the largest mean diameter, 61.2 ± 1.1 nm (mean± SEM, n=178) compared to the other samples (Student's t-test, $p< 0.001$) (Fig 2). The larger diameter can be explained by flattening of the vesicles upon drying down in the negative stain.

Molecular Structure of Synaptic Vesicles

Knob-like protrusions found on the surfaces of SV, apparent after negative staining, have previously been regarded as the vacuolar ATP-dependent proton pump (V-ATPase) (Takamori *et al.*, 2006, Wilkens *et al.*, 2005). V-ATPases are large, membrane bound multi subunit complexes that translocate protons across membranes. The number of V-ATPase structures per vesicle was variable, with most vesicles containing four or five (Fig 3). Correlation analysis failed to detect a linear relationship between vesicle size and V-ATPase number (data not shown). Guinea pig (Stadler and Tsukita, 1984) and rat (Takamori et al., 2006) synaptic vesicles contains one or two, and occasionally three or four V-ATPase per

vesicle. Although the density of V-ATP structures in squid SV is greater than reported values, the size of the individual units, 15-20 nm in diameter, is in good agreement.

Electron microscopy of synaptic vesicles negative stained with Nano-W served to further evaluate molecular structures at SV surfaces. The negative stain methylamine tungstate tolerates collection of 140 images typically needed for a tomography series, yielding reconstructions of SV surfaces with exquisite detail. Seven tomograms, corresponding to ten vesicles, were examined and analyzed in virtual sections calculated from tomograms. Overlap of images of individual proteins on the surfaces of the synaptic vesicles is eliminated by the calculation of virtual sections along three arbitrary perpendicular axes (Kremer et al., 1996). Surfaces of vesicles, as expected, displayed numerous structures presumed to be proteins. There are no indications from measurements of diameters that stain penetrates inside SVs, suggesting that the mixture of proteins and lipids on the surface of SV is not affected by the processing for electron microscopy. Therefore, the protein coat of the synaptic vesicle appears to be distributed uniformly on its surface rather than tight clusters within restricted domains as reported previously (Bennett *et al.*, 1992), since we do not see open membrane patches. One exception to this appearance of distribution is the few much larger surface components displaying a size and shape consistent with the V-ATPase (Fig 3).

Squid V-ATPase showed structural similarity to its mammalian homologues (Takamori *et al.*, 2006, Wilkens *et al.*, 2005). There are very few sequences corresponding to squid proteins in public databases, but squid data (DeGiorgis et al., in press) containing 23,000 ESTs from *Loligo pealei* were used to search for nucleotide sequences corresponding to the V-ATPase peptides. The tBLASTn algorithm running locally pinpointed 10 EST that showed significant, but not exact, alignment cross species (Table 2). Conserved domains in V-ATPase subunits, are thus in agreement with the observed structural homology.

Discussion

Dowdall and Whittaker described the isolation of a synaptic vesicle rich fraction from squid optic lobe (Dowdall and Whittaker, 1973). However, the purity of the SV-rich fraction was not evaluated by either biochemical or electron microscopy techniques. Subsequently, SVs purified by this method from frozen squid optic lobe with the additional purification step of controlled-pore glass chromatography yielded a purity of approximately 60% (Chin and Goldman, 1992). Since rat brain SV can be purified to >95% purity (Huttner et al., 1983) we modified this purification scheme for rat brain to isolate highly pure SV's from fresh squid optic lobes. Determinations of SV size distributions in SV-enriched fractions suggests that this isolation protocol provides >95% pure synaptic vesicles from squid optic lobes.

The results presented here clearly demonstrate that the estimates of SV size are dependent upon the method of preparation of the SV sample for EM. Section thickness is unlikely to be a source of variation because we only measured vesicles for which the delimiting edges of the membrane were visible in a single section and then computed the size based on ferrets diameter with a circularity value close to unity. Fixation and processing conditions can alter the absolute dimensions of organelles (Fox, 1988, Tatsuoka and Reese, 1989). In mammalian cholinergic synapses, the rapid frozen, freeze-substituted SV diameter is also significantly greater than those obtained by aldehyde-fixation, presumably because the osmotic effects of fixatives are avoided (Tatsuoka and Reese, 1989). We think that our use of osmotically balanced solutions in the SV isolation was important to have the diameter of the frozen, freeze-substituted isolated SV to match those found in frozen intact nerve endings. Negative stained, non-fixed isolated SV samples had the largest mean diameter relative to the other samples obtained by different preparation techniques. It should be kept in mind that the negative stain image is a projection of the whole vesicle while the sections

are often only part of a vesicle and not every instance include the section from the equator. It is also known that when protein-containing lipid vesicles are negatively stained, these vesicles dry down and collapse by approaching the diameter of two discs with the same area, one on top, one below (Peter, 2010, Szoka and Papahadjopoulos, 1980). Changes in vesicle shape from spheres to disk by negative staining would explain the significant increase in negative stained SV diameter that we observed.

Indeed such flattening is directly demonstrated in the tomographic reconstructions here (Fig 3A, inset). With this method, SV membranes appear to be uniformly coated with structures – big knobs and smaller hairs, ostensibly the knobs are the V- ATPase standing out because it is much larger than other SV proteins. Because the stain does not get inside the vesicle, its membrane is not enclosed on both sides, and it is poorly outlined by negative stain in XZ projections of tomograms, so the membrane appears only as a faint boundary between stain and non-stain. The upper and lower boundaries of vesicles, due to the hair-like structures, are hard to see *except* where the boundary is decorated by knobs. Here, the knobs clearly delineate the position of the membrane at that point. Thus, knobs on vesicle membranes near the centers of vesicles appear to be on a flat surface suspended across the ends of the vesicles, like the top of a drum, rather than perched on domes, showing that the vesicles are flattened and actually a little thicker at their edges where their membranes fold back on themselves.

It remains to be determined the degree to which detergents used for vesicle isolation in previously published methods, and the specificity of metal-protein surface interactions implicit to the negative staining procedure, affect the organization of proteins on the SV surface. We demonstrate here three-dimensional molecular reconstructions based on tomograms from single intact synaptic vesicles isolated without detergents. The tomograms are obtained by negative stain based electron microscopy, which permits imaging free from the assumptions of symmetry, classification, and averaging. While further research is needed to determine if proteins of specific type may cluster with each other in restricted domains (Bennett *et al.*, 1992), below the structures noted above, negative staining tomography shows a continuous layer of protein blanketing the surfaces of synaptic vesicles.

In summary, we have optimized the routine collection of relatively large quantities of highly purified synaptic vesicles and performed negative staining tomography, to investigate the distribution of molecules on their surfaces. Importantly, the vesicle flattening we detect is likely to result in artifactually enlarged radii of curvature if negative staining is the only measure of diameter in vesicular and tubular systems.

Acknowledgments

We are grateful to Jane Farrington for examining fractions in the electron microscope, and Dr. Harish Pant for teaching us the optic lobe dissection and homogenization. JAD is supported by the RI-INBRE program award # P20RR016457-10 from the National Center for Research Resources (NCRR), NIH.

References

Bennett MK, Calakos N, Kreiner T, Scheller RH. Synaptic vesicle membrane proteins interact to form a multimeric complex. J. Cell Biol. 1992; 116:761–775. [PubMed: 1730776]

Bernal RA, Stock D. Three-dimensional structure of the intact Thermus thermophilus H+-ATPase/synthase by electron microscopy. Structure. 2004; 12:1789–1798. [PubMed: 15458628]

Carlson SS, Wagner JA, Kelly RB. Purification of synaptic vesicles from elasmobranch electric organ and the use of biophysical criteria to demonstrate purity. Biochemistry (Mosc). 1978; 17:1188–1199.

Chin GJ, Goldman SA. Purification of squid synaptic vesicles and characterization of the vesicle-associated proteins synaptobrevin and Rab3A. Brain Res. 1992; 571:89–96. [PubMed: 1319264]

Clift-O'Grady L, Linstedt AD, Lowe AW, Grote E, Kelly RB. Biogenesis of synaptic vesicle-like structures in a pheochromocytoma cell line PC-12. J. Cell Biol. 1990; 110:1693–1703. [PubMed: 2110571]

Dowdall MJ, Whittaker VP. Comparative studies in synaptosome formation: the preparation of synaptosomes from the head ganglion of the squid, Loligo pealii. J. Neurochem. 1973; 20:921–935. [PubMed: 4697892]

Fox GQ. A morphometric analysis of synaptic vesicle distributions. Brain Res. 1988; 475:103–117. [PubMed: 3214719]

Huttner WB, Schiebler W, Greengard P, De Camilli P. Synapsin I (protein I), a nerve terminal-specific phosphoprotein. III. Its association with synaptic vesicles studied in a highly purified synaptic vesicle preparation. J. Cell Biol. 1983; 96:1374–1388. [PubMed: 6404912]

Kremer JR, Mastronarde DN, McIntosh JR. Computer visualization of three-dimensional image data using IMOD. J. Struct. Biol. 1996; 116:71–76. [PubMed: 8742726]

Kretzschmar S, Volknandt W, Zimmermann H. Colocalization on the same synaptic vesicles of syntaxin and SNAP-25 with synaptic vesicle proteins: a re-evaluation of functional models required? Neurosci. Res. 1996; 26:141–148. [PubMed: 8953576]

Peter, B. Negative-stain spreading of protein-protein and protein-lipid complexes for EM. McMahon Lab, Neurobiology Division, MRC Lab of Molecular Biology; 2010. http://www.endocytosis.org/techniqs/Negative%20stain%20protocol.html

Petersen JD, Chen X, Vinade L, Dosemeci A, Lisman JE, Reese TS. Distribution of postsynaptic density (PSD)-95 and Ca2+/calmodulin-dependent protein kinase II at the PSD. J. Neurosci. 2003; 23:11270–11278. [PubMed: 14657186]

Pollard HB, Banker JL, Bohr WA, Dowdall MJ. Chlorpromazine: Specific inhibition of L-noradrenaline and 5-hydroxytryptamine uptake in synaptosomes from squid brain. Brain Res. 1975; 85:23–31.

Stadler H, Tsukita S. Synaptic vesicles contain an ATP-dependent proton pump and show ‘knob-like’ protrusions on their surface. EMBO J. 1984; 3:3333–3337. [PubMed: 6151900]

Szoka F Jr. Papahadjopoulos D. Comparative properties and methods of preparation of lipid vesicles (liposomes). Annu. Rev. Biophys. Bioeng. 1980; 9:467–508. [PubMed: 6994593]

Takamori S, Holt M, Stenius K, Lemke EA, Gronborg M, Riedel D, Urlaub H, Schenck S, Brugger B, Ringler P, Muller SA, Rammner B, Grater F, Hub JS, De Groot BL, Mieskes G, Moriyama Y, Klingauf J, Grubmuller H, Heuser J, Wieland F, Jahn R. Molecular anatomy of a trafficking organelle. Cell. 2006; 127:831–846. [PubMed: 17110340]

Tatsuoka H, Reese TS. New structural features of synapses in the anteroventral cochlear nucleus prepared by direct freezing and freeze-substitution. J. Comp. Neurol. 1989; 290:343–357. [PubMed: 2592616]

Wilkens S, Zhang Z, Zheng Y. A structural model of the vacuolar ATPase from transmission electron microscopy. Micron. 2005; 36:109–126. [PubMed: 15629643]

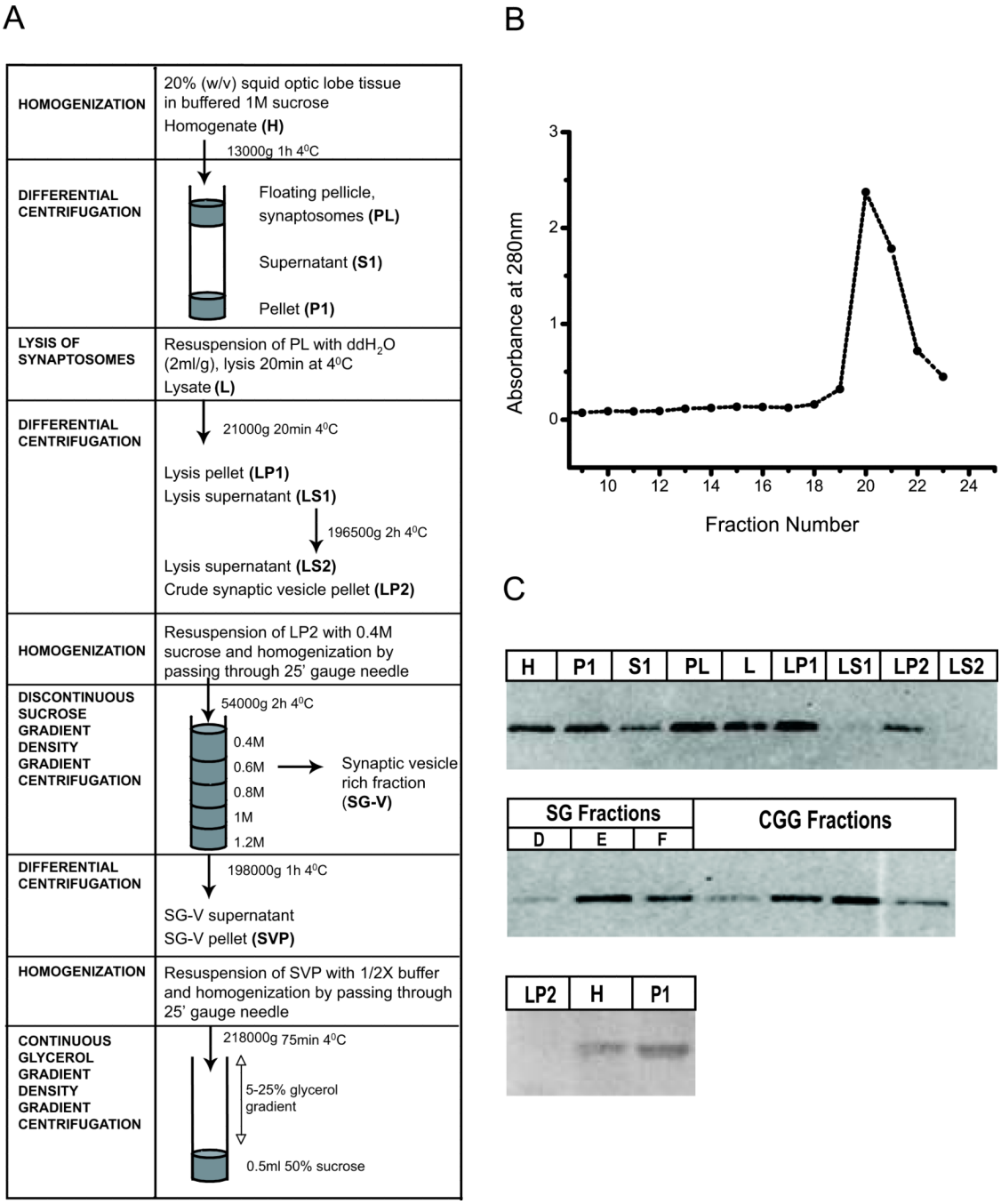

Figure 1.

Synaptic vesicle enrichment by glycerol velocity sedimentation. (A) Scheme summarizing purification of synaptic vesicles from squid optic lobes. (B) Glycerol gradient fractions (250ml) collected from top to bottom and analyzed for their absorbance at 280nm. Major peak indicates synaptic vesicle rich fraction. (C) Electron micrograph of synaptic vesicle rich fraction (D) Western blot of subcellular fractions obtained during the synaptic vesicle purification steps (as described in Materials and Method) with mitochondrial marker; Anti-VDAC (40μg protein/lane) and synaptic marker Anti-SNAP25 (5μg protein/lane) antibodies.

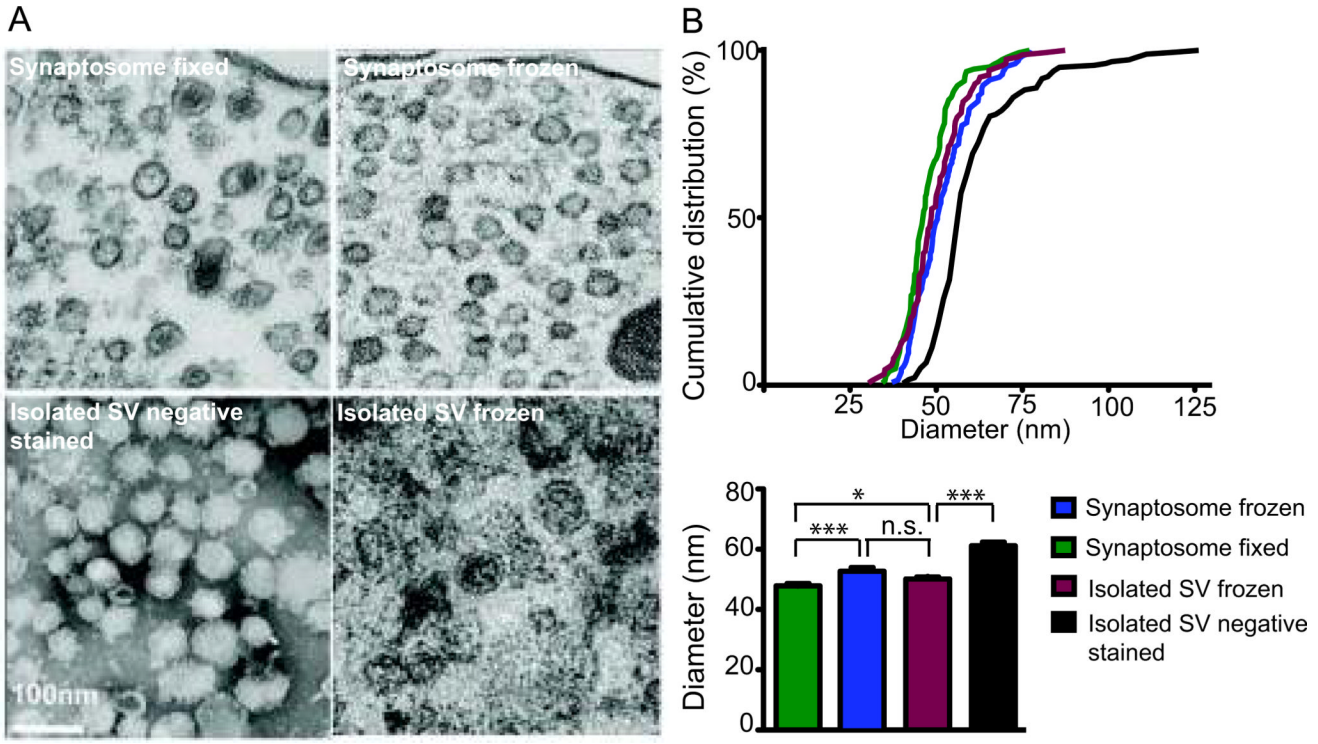

Figure 2.

Comparison of squid synaptic vesicle (SV) size by altering electron microscopy sample preparation technique in synaptosomes and isolated vesicles. (A) Electron micrograph of (left to right) fixed, embedded, thin-sectioned synaptosome; slam-frozen, freeze substituted synaptosome; negative stained isolated SVs and slam-frozen, freeze substituted isolated synaptic vesicles. (B) Cumulative distribution of synaptic vesicle diameters. Variations in mean synaptic vesicle diameter due to different sample preparation regimens (mean ± SEM, n= 125-175, Student's t-test; “*” = p< 0.03, “***” = p<0.001, n.s. = not significant).

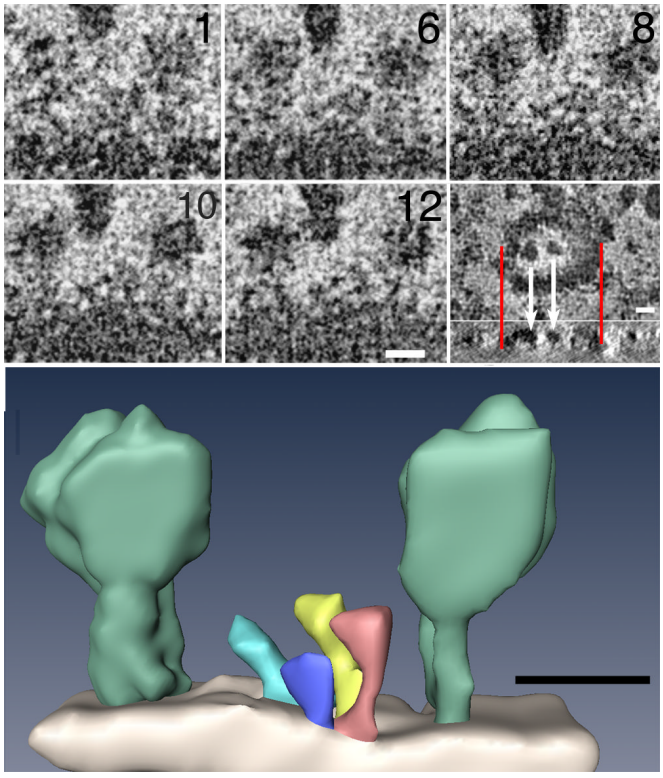

Figure 3.

(A) Five virtual sections, each 0.6 nm thick, extracted from different levels in a tomogram of a single negative stained synaptic vesicle. The external surface of the vesicle displays three prominent molecules (arrow). Synaptic vesicles collapse during negative staining, leaving other prominent molecules (arrowhead) on their collapsed external surfaces exposed to negative stain. Data have been adjusted for brightness and contrast, binned by two and spatially filtered to increase the signal-to-noise (S/N). Inset (lower right panel): Virtual section through vesicle in en-face plane showing how two large surface particles (white arrows) aligned with a cross sectional projection below. Red lines delineate two edges of vesicle above and the same edges below. Surface particles lie in a plane defined by the two edges of the vesicle, showing that the vesicle is flattened onto the substrate (below). (Scale bar = 10 nm). (B) Corresponding surface rendering of structures on the surface of the vesicle in A, including two of the more prominent ones (light green) whose sizes and shapes correspond to EM reconstructions of the V-ATPase of *T. Thermophilus* (Bernal and Stock, 2004). Smaller structures (other colors) are also evident on the surface of the vesicle. (Scale bar = 10 nm).

Table 1

Distribution of Protein and % Recovery in Subcellular Fractions Obtained in the Course of Purification of Synaptic Vesicles from Squid Optic Lobe (11g optic lobe tissue, mean ± SD, n=4).

Subcellular Fraction	Total Protein	
	Amount (mg)	Recovery (%)
H	1041.45 ± 184.68	100.00
PL	144.28 ± 84.22	16.91 ± 1.75
S1	318.04 ± 50.94	30.61 ± 1.02
P1	354.14 ± 73.06	34.7 ± 9.26
L	201.01 ± 55.25	18.72 ± 3.43
LP1	100.08 ± 23.91	10.03 ± 3.46
LS1	44.46 ± 10.31	4.39 ± 1.4
LP2	8.91 ± 2.22	0.89 ± 0.33
LS2	32.55 ± 5.41	3.19 ± 0.67
SG-E	2.78 ± 3.54	0.27 ± 0.38
SG-F	2.1 ± 0.72	0.21 ± 0.1
SG-E supernatant	1.13 ± 1.56	0.12 ± 0.17
CGG-19	0.17 ± 0.02	0.02 ± 0
CGG-20	0.32 ± 0.13	0.03 ± 0.01
CGG-21	0.25 ± 0.2	0.02 ± 0.02

Table 2

Cross species sequence comparisons of V-ATPase transcripts identified in squid neuronal tissues.

Top Blastx	Accession No. Species	Match Loc	Id/Sim %
V_1 Catalytic Subunit a	Q7sy46 zebrafish	13-266	80/90
V_1 Catalytic Subunit a	Q90647 chick	404617*	81/92
V_1 Catalytic Subunit c	Q291s7 fruitfly	1-229	61/76
V_1 Subunit d	Q6azj2 frog	5-192	79/91
V_1 Subunit e	Qhqt6 mosquito	1-224	67/82
V_1 Subunit g	Q59gy4 oyster	7-60	55/57
V_1 Subunit h	Q7qg40 mosquito	228-447	67/80
V_1 Subunit h	Q7qg40 mosquito	4-210	56/76
V_0 16 kd proteolipid subunit c	Q6p041 zebrafish	1-153	77/83
V_0 21 kd proteolipid subunit c	Q6pd81 zebrafish	2-203	67/79